



HAL
open science

Arbitrary order monotonic finite-volume schemes for 2D elliptic problems

Xavier Blanc, Francois Hermeline, Emmanuel Labourasse, Julie Patela

► To cite this version:

Xavier Blanc, Francois Hermeline, Emmanuel Labourasse, Julie Patela. Arbitrary order monotonic finite-volume schemes for 2D elliptic problems. 2023. cea-04211874

HAL Id: cea-04211874

<https://cea.hal.science/cea-04211874>

Preprint submitted on 20 Sep 2023

HAL is a multi-disciplinary open access archive for the deposit and dissemination of scientific research documents, whether they are published or not. The documents may come from teaching and research institutions in France or abroad, or from public or private research centers.

L'archive ouverte pluridisciplinaire **HAL**, est destinée au dépôt et à la diffusion de documents scientifiques de niveau recherche, publiés ou non, émanant des établissements d'enseignement et de recherche français ou étrangers, des laboratoires publics ou privés.

Arbitrary order monotonic finite-volume schemes for 2D elliptic problems

Xavier Blanc¹, Francois Hermeline^{2,3}, Emmanuel Labourasse^{2,3}, and Julie Patela^{1,2}

¹Université Paris Cité, Sorbonne Université, CNRS, Laboratoire Jacques-Louis Lions, F-75013 Paris, France.

²CEA, DAM, DIF, F-91297 Arpajon, France.

³Université Paris-Saclay, CEA DAM DIF, Laboratoire en Informatique Haute Performance pour le Calcul et la Simulation, 91297 Arpajon, France.

September 20, 2023

Abstract

Monotonicity is very important in most applications solving elliptic problems. Many schemes preserving positivity has been proposed but are at most second-order convergent. Besides, in general, high-order schemes do not preserve positivity. In the present paper, we propose an arbitrary-order monotonic method for elliptic problems in 2D. We show how to adapt our method to the case of a discontinuous and/or tensor-valued diffusion coefficient, while keeping the order of convergence. We assess the new scheme on several test problems.

Keywords— Finite volume method, elliptic problem, anisotropic diffusion, monotonicity, high order

Contents

1	Introduction	2
2	Definitions and notations	3
3	Finite volume formulation	3
3.1	Approximation of the interior fluxes	3
3.2	Approximation of the boundary fluxes	6
3.2.1	Neumann boundary condition	6
3.2.2	Dirichlet boundary condition	7
3.3	High-order reconstruction by interpolation	7
4	Monotonicity	8
4.1	Matrix form	8
4.2	Picard iteration method	9
5	Properties	9
5.1	Conservation	9
5.2	Monotonicity	10
5.3	Well-posedness of the Picard iteration method	10
6	Numerical experiments	11
6.1	Numerical accuracy assessment	12
6.1.1	Discontinuous diffusion coefficient	12
6.1.2	Anisotropic diffusion coefficient	12
6.2	Monotonicity assessment	15
6.2.1	Tensor-valued coefficient κ and square domain with a square hole	15
6.2.2	Fokker-Planck type diffusion equation	17
7	Concluding remarks	17

1 Introduction

This paper describes a follow-up of two recently published works [6, 7]. In the former work, we designed a monotonic and arbitrary-order numerical method for an elliptic equation in 1D. In the latter one, we showed that the approach used in 1D extends to second-order accurate methods in 2D. Our goal in this paper is to propose the first arbitrary-order monotonic method for elliptic problems in 2D.

The model we consider is

$$\begin{cases} -\nabla \cdot (\boldsymbol{\kappa} \nabla \bar{u}) + \lambda \bar{u} = f & \text{in } \Omega, \\ \bar{u} = g_D & \text{on } \Gamma_D, \\ \boldsymbol{\kappa} \nabla \bar{u} \cdot \mathbf{n} = g_N & \text{on } \Gamma_N, \end{cases} \quad (1)$$

where Ω is a bounded open domain of \mathbb{R}^2 with $\partial\Omega = \Gamma_D \cup \Gamma_N$ ($\Gamma_D \cap \Gamma_N = \emptyset$), and $\mathbf{n} \in \mathbb{R}^2$ is the outgoing unit normal vector. The data are such that $f \in L^2(\Omega)$, $g_D \in H^{1/2}(\Gamma_D)$, $g_N \in L^2(\Gamma_N)$, $\lambda \in \mathbb{R}^+$ (if $\lambda = 0$, then $|\Gamma_D| > 0$), and $\boldsymbol{\kappa} \in L^\infty(\Omega)$. The tensor-valued diffusion coefficient $\boldsymbol{\kappa}$ satisfies the uniform ellipticity condition:

$$\forall \mathbf{x} \in \Omega, \forall \boldsymbol{\xi} \in \mathbb{R}^2, \quad \kappa_{\min} \|\boldsymbol{\xi}\|^2 \leq \boldsymbol{\xi}^t \boldsymbol{\kappa}(\mathbf{x}) \boldsymbol{\xi}. \quad (2)$$

where κ_{\min} is a strictly positive coefficient. Under the above conditions, one can prove (using Lax-Milgram Lemma in the spirit of [19], Chapter 6) that system (1) has a unique solution in $H^1(\Omega)$ which satisfies a positiveness principle, i.e. if $f \geq 0$ and $g \geq 0$, then $\bar{u} \geq 0$. One often refers to monotonicity in the literature for this principle.

For the applications we have in mind, such as inertial confinement fusion simulations, we need to be able to solve problem (1) on (almost) arbitrary meshes. The reason for this is twofold. First, the domain Ω can be very distorted. Second, problem (1) is coupled to the incompressible Euler system, which is discretized using a Lagrangian finite volume scheme (see [13, 24, 27]). We thus have no control on the quality of the mesh. Further, a fundamental property of the hydrodynamics scheme is to be conservative, in order to reproduce as precisely as possible singular solutions, such as shocks. Thus, the diffusion scheme applied to (1) should be conservative too, in order to preserve this property. As a consequence, monotonicity cannot be recovered by merely truncating negative values: such a strategy is incompatible with conservativity.

This is why a large amount of work has been devoted to the design of monotone schemes since the seminal works of [5, 26]. Among other publications, let us cite recent works [11, 12, 30, 32, 34, 36, 37, 40] and references therein about this topic. However, none of these methods is arbitrarily high-order accurate. The most advanced work in this direction is [37], which achieved third-order accuracy.

Some methods are particularly well-suited for achieving arbitrary high-order for elliptic problems. Let us cite for instance the finite-element method [14], the Virtual Element method [4], the Discontinuous Galerkin method [15], and the Hybrid High-Order method [16]. However, very few (see [2, 3, 10, 35] and references therein) can enforce the positiveness of the unknown without imposing severe constraints on the mesh, and none of them achieve a convergence order higher than two. Another reason for not using these methods in our context, is that their coupling with other models can be problematic since the degrees of freedom of the different discrete operators approximations do not match.

This work proposes the first arbitrary-order monotonic scheme for the elliptic equation (1). The diffusion coefficient can be tensor-valued and/or discontinuous. We show that we preserve the arbitrary high-order accuracy even with a discontinuous diffusion coefficient as long as discontinuities are known and coincide with edges of the mesh. We recall the main steps of the proposed method (see also [7]):

1. Integration of the equation over each cell of the mesh.
2. Transformation of this surface integral into a sum of fluxes using the divergence theorem.
3. Approximation of the fluxes using a Gauss quadrature rule on each edge of the cell.
4. Taylor expansion of the solution \bar{u} in the neighborhood of each Gauss quadrature point of each edge along *two* independent privileged directions in order to obtain an approximation of $\nabla \bar{u}$ involving the values of \bar{u} and its derivatives at certain suitably chosen points, in this case the center of mass and vertices of the cell.
5. Using this Taylor expansion, estimation of $(\boldsymbol{\kappa} \nabla \bar{u}) \cdot \mathbf{n} = (\nabla \bar{u}) \cdot (\boldsymbol{\kappa}^t \mathbf{n})$.
6. Calculation of the values of \bar{u} at vertices by a polynomial interpolation formula in the neighborhood of the Gauss quadrature points of each cell edge.
7. Calculation of the values of derivatives of \bar{u} at centers of mass and vertices of the neighboring cells by differentiating this polynomial interpolation.
8. Transformation of the scheme into a monotonic non-linear two-point flux approximation.

9. Resolution of the non-linear system by the Picard iteration method.

The paper is structured as follows. Definitions and notations are given in Section 2. The proposed arbitrarily high-order Finite-Volume method is described in Section 3. Then, we explain how the scheme is modified to enforce the monotonicity in Section 4. In Section 5, we prove some nice properties of the method. Finally the arbitrary high-order accuracy and the monotonicity of the method are assessed in Section 6 on some classical benchmarks including cases with anisotropic and discontinuous diffusion coefficients.

2 Definitions and notations

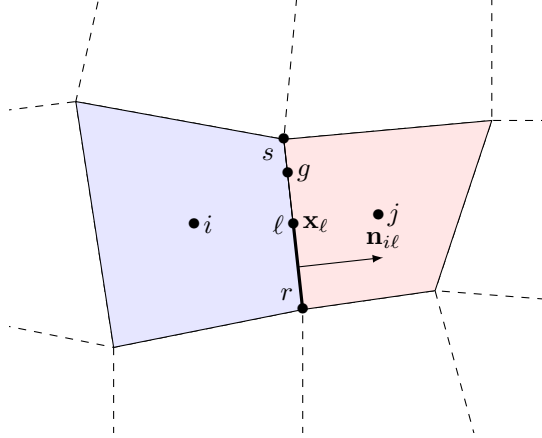


Figure 1: Example of a mesh with our notations.

Given an arbitrary mesh the cells of which are numbered from 1 to n , consider a cell denoted i and its neighbor j (see Figure 1). The center of mass of i (resp. j) is denoted by \mathbf{x}_i (resp. \mathbf{x}_j), their common edge is ℓ and the vertices of ℓ are \mathbf{x}_r and \mathbf{x}_s . The position of the center of the edge ℓ is \mathbf{x}_ℓ . We denote by \mathbf{x}_g a Gauss quadrature point located on the edge ℓ . The length of ℓ is $|\ell|$ and the volume of a cell i is V_i . The normal vector $\mathbf{n}_{i\ell}$ is the unit vector which is orthogonal to the edge ℓ and outgoing for the cell i . We define $h = \min_{\ell} |\ell|$.

Given $\mathbf{v} = (v_i)$ a vector in \mathbb{R}^n we will denote respectively its Euclidian, L^2 and L^∞ norms by

$$\|\mathbf{v}\| = \left(\sum_{i=1}^n v_i^2 \right)^{1/2}, \quad \|\mathbf{v}\|_2 = \left(\sum_{i=1}^n V_i v_i^2 \right)^{1/2}, \quad \|\mathbf{v}\|_\infty = \max_{1 \leq i \leq n} |v_i|$$

and we use the notation $\mathbf{v} > \mathbf{0}$ (resp. $\mathbf{v} \geq \mathbf{0}$) if, for all i , $v_i > 0$ (resp. $v_i \geq 0$).

3 Finite volume formulation

To simplify the presentation we suppose that κ is isotropic : $\kappa = \kappa \mathbf{I}$, with $\kappa > \kappa_{\min}$. It is worth noting that the full anisotropic case can be immediately dealt with by remarking that $(\kappa \nabla \bar{u}) \cdot \mathbf{n} = (\nabla \bar{u}) \cdot (\kappa^t \mathbf{n})$ and by replacing \mathbf{n} by $\kappa^t \mathbf{n}$ in what follows. Moreover we assume that the discontinuities of κ coincide with edges of the mesh.

3.1 Approximation of the interior fluxes

The first step to design a finite volume scheme consists in integrating (1) on cell i

$$-\int_i \nabla \cdot \kappa \nabla \bar{u} + \int_i \lambda \bar{u} = \int_i f.$$

Thanks to the divergence formula we obtain

$$-\sum_{\ell \in i} \int_\ell \kappa \nabla \bar{u} \cdot \mathbf{n} + \int_i \lambda \bar{u} = \int_i f. \quad (3)$$

Using a k -th order accurate Gauss's quadrature formula for approximating the flux through the edge ℓ

$$\bar{\mathcal{F}}_\ell = \int_\ell \kappa \nabla \bar{u} \cdot \mathbf{n}$$

we have

$$-\sum_{\ell \in i} |\ell| \sum_{g \in \ell} \omega_g \kappa(\mathbf{x}_g) (\nabla \bar{u})(\mathbf{x}_g) \cdot \mathbf{n}_{i\ell} + \int_i \lambda \bar{u} = \int_i f + \mathcal{O}(h^k),$$

where ω_g and \mathbf{x}_g are respectively the weights and the points of the quadrature. Thus we have to approximate

$$\kappa(\mathbf{x}_g) (\nabla \bar{u})(\mathbf{x}_g) \cdot \mathbf{n}_{i\ell}.$$

Suppose that $\bar{u} \in W^{1,\infty}(\Omega)$ and denote :

$$N_q^p = \frac{1}{p!} \binom{p}{q} = \frac{1}{q!(p-q)!}.$$

A Taylor expansion at order k in the neighborhood of \mathbf{x}_g gives

$$\bar{u}(\mathbf{x}) = \bar{u}(\mathbf{x}_g) + (\mathbf{x} - \mathbf{x}_g) \cdot \nabla \bar{u}(\mathbf{x}_g) + \sum_{p=2}^k \sum_{q=0}^p N_q^p \frac{\partial^p \bar{u}}{\partial x^q \partial y^{p-q}}(\mathbf{x}_g) (x - x_g)^q (y - y_g)^{p-q} + \mathcal{O}(\|\mathbf{x} - \mathbf{x}_g\|^{k+1}). \quad (4)$$

Denote by \bar{u}_i the mean value of u in cell i

$$\bar{u}_i = \frac{1}{V_i} \int_i \bar{u}(\mathbf{x}) dx.$$

Integrating (4) on cells i, j and dividing respectively by their volume V_i, V_j provides

$$\bar{u}_i = \bar{u}(\mathbf{x}_g) + (\mathbf{x}_i - \mathbf{x}_g) \cdot \nabla \bar{u}(\mathbf{x}_g) + \frac{1}{V_i} \sum_{p=2}^k \sum_{q=0}^p N_q^p \frac{\partial^p \bar{u}}{\partial x^q \partial y^{p-q}}(\mathbf{x}_g) \int_i (x - x_g)^q (y - y_g)^{p-q} dx + \mathcal{O}(h^{k+1}),$$

$$\bar{u}_j = \bar{u}(\mathbf{x}_g) + (\mathbf{x}_j - \mathbf{x}_g) \cdot \nabla \bar{u}(\mathbf{x}_g) + \frac{1}{V_j} \sum_{p=2}^k \sum_{q=0}^p N_q^p \frac{\partial^p \bar{u}}{\partial x^q \partial y^{p-q}}(\mathbf{x}_g) \int_j (x - x_g)^q (y - y_g)^{p-q} dx + \mathcal{O}(h^{k+1}).$$

hence

$$(\mathbf{x}_g - \mathbf{x}_i) \cdot \nabla \bar{u}(\mathbf{x}_g) = \bar{u}(\mathbf{x}_g) - \bar{u}_i + \bar{r}_{gi},$$

$$(\mathbf{x}_j - \mathbf{x}_g) \cdot \nabla \bar{u}(\mathbf{x}_g) = \bar{u}_j - \bar{u}(\mathbf{x}_g) + \bar{r}_{gj}$$

with

$$\bar{r}_{gi} = \frac{1}{V_i} \sum_{p=2}^k \sum_{q=0}^p N_q^p \frac{\partial^p \bar{u}}{\partial x^q \partial y^{p-q}}(\mathbf{x}_g) \int_i (x - x_g)^q (y - y_g)^{p-q} dx + \mathcal{O}(h^{k+1}),$$

$$\bar{r}_{gj} = -\frac{1}{V_j} \sum_{p=2}^k \sum_{q=0}^p N_q^p \frac{\partial^p \bar{u}}{\partial x^q \partial y^{p-q}}(\mathbf{x}_g) \int_j (x - x_g)^q (y - y_g)^{p-q} dx + \mathcal{O}(h^{k+1})$$

Using respectively $\mathbf{x} = \mathbf{x}_r$ and $\mathbf{x} = \mathbf{x}_s$ in the Taylor expansion (4), we obtain

$$\bar{u}(\mathbf{x}_r) = \bar{u}(\mathbf{x}_g) + (\mathbf{x}_r - \mathbf{x}_g) \cdot \nabla \bar{u}(\mathbf{x}_g) + \sum_{p=2}^k \sum_{q=0}^p N_q^p \frac{\partial^p \bar{u}}{\partial x^q \partial y^{p-q}}(\mathbf{x}_g) (x_r - x_g)^q (y_r - y_g)^{p-q} + \mathcal{O}(h^{k+1}),$$

$$\bar{u}(\mathbf{x}_s) = \bar{u}(\mathbf{x}_g) + (\mathbf{x}_s - \mathbf{x}_g) \cdot \nabla \bar{u}(\mathbf{x}_g) + \sum_{p=2}^k \sum_{q=0}^p N_q^p \frac{\partial^p \bar{u}}{\partial x^q \partial y^{p-q}}(\mathbf{x}_g) (x_s - x_g)^q (y_s - y_g)^{p-q} + \mathcal{O}(h^{k+1}).$$

Subtracting these equalities gives

$$(\mathbf{x}_s - \mathbf{x}_r) \cdot \nabla \bar{u}(\mathbf{x}_g) = \bar{u}(\mathbf{x}_s) - \bar{u}(\mathbf{x}_r) + \bar{r}_{rs}$$

with

$$\bar{r}_{rs} = - \sum_{p=2}^k \sum_{q=0}^p N_q^p \frac{\partial^p \bar{u}}{\partial x^q \partial y^{p-q}}(\mathbf{x}_g) ((x_s - x_g)^q (y_s - y_g)^{p-q} - (x_r - x_g)^q (y_r - y_g)^{p-q}) + \mathcal{O}(h^{k+1}).$$

Thus, we have the system

$$\begin{cases} \nabla \bar{u}(\mathbf{x}_g) \cdot (\mathbf{x}_g - \mathbf{x}_i) = \bar{u}(\mathbf{x}_g) - \bar{u}_i + \bar{r}_{gi}, \\ \nabla \bar{u}(\mathbf{x}_g) \cdot (\mathbf{x}_j - \mathbf{x}_g) = \bar{u}_j - \bar{u}(\mathbf{x}_g) + \bar{r}_{gj}, \\ \nabla \bar{u}(\mathbf{x}_g) \cdot (\mathbf{x}_s - \mathbf{x}_r) = \bar{u}(\mathbf{x}_s) - \bar{u}(\mathbf{x}_r) + \bar{r}_{rs}. \end{cases} \quad (5)$$

We can decompose the unit normal vector $\mathbf{n}_{i\ell}$ both in the basis $((\mathbf{x}_g - \mathbf{x}_i), (\mathbf{x}_s - \mathbf{x}_r))$ and $((\mathbf{x}_j - \mathbf{x}_g), (\mathbf{x}_s - \mathbf{x}_r))$

$$\mathbf{n}_{i\ell} = \alpha_{gi} \frac{\mathbf{x}_g - \mathbf{x}_i}{\|\mathbf{x}_g - \mathbf{x}_i\|} + \beta_{gi} \frac{\mathbf{x}_s - \mathbf{x}_r}{\|\mathbf{x}_s - \mathbf{x}_r\|} = \alpha_{gj} \frac{\mathbf{x}_j - \mathbf{x}_g}{\|\mathbf{x}_j - \mathbf{x}_g\|} + \beta_{gj} \frac{\mathbf{x}_s - \mathbf{x}_r}{\|\mathbf{x}_s - \mathbf{x}_r\|}$$

with

$$\alpha_{gi} = \frac{\|\mathbf{x}_g - \mathbf{x}_i\|}{(\mathbf{x}_g - \mathbf{x}_i) \cdot \mathbf{n}_{i\ell}} \geq 0, \quad (6)$$

$$\beta_{gi} = \frac{\|\mathbf{x}_s - \mathbf{x}_r\| \mathbf{n}_{i\ell} \cdot (\mathbf{x}_g - \mathbf{x}_i)^\perp}{(\mathbf{x}_s - \mathbf{x}_r) \cdot (\mathbf{x}_g - \mathbf{x}_i)^\perp} \quad (7)$$

and

$$\alpha_{gj} = \frac{\|\mathbf{x}_j - \mathbf{x}_g\|}{(\mathbf{x}_j - \mathbf{x}_g) \cdot \mathbf{n}_{i\ell}} \geq 0,$$

$$\beta_{gj} = \frac{\|\mathbf{x}_s - \mathbf{x}_r\| \mathbf{n}_{i\ell} \cdot (\mathbf{x}_j - \mathbf{x}_g)^\perp}{(\mathbf{x}_s - \mathbf{x}_r) \cdot (\mathbf{x}_j - \mathbf{x}_g)^\perp}.$$

Thus, we have the expression of the gradient in the direction of the normal vector seen by the cell i, j , respectively denoted by $\nabla \bar{u}(\mathbf{x}_g)_i \cdot \mathbf{n}_{i\ell}$, $\nabla \bar{u}(\mathbf{x}_g)_j \cdot \mathbf{n}_{i\ell}$

$$\nabla \bar{u}(\mathbf{x}_g)_i \cdot \mathbf{n}_{i\ell} = \alpha_{gi} \frac{\nabla \bar{u}(\mathbf{x}_g) \cdot (\mathbf{x}_g - \mathbf{x}_i)}{\|\mathbf{x}_g - \mathbf{x}_i\|} + \beta_{gi} \frac{\nabla \bar{u}(\mathbf{x}_g) \cdot (\mathbf{x}_s - \mathbf{x}_r)}{\|\mathbf{x}_s - \mathbf{x}_r\|}, \quad (8)$$

$$\nabla \bar{u}(\mathbf{x}_g)_j \cdot \mathbf{n}_{i\ell} = \alpha_{gj} \frac{\nabla \bar{u}(\mathbf{x}_g) \cdot (\mathbf{x}_j - \mathbf{x}_g)}{\|\mathbf{x}_j - \mathbf{x}_g\|} + \beta_{gj} \frac{\nabla \bar{u}(\mathbf{x}_g) \cdot (\mathbf{x}_s - \mathbf{x}_r)}{\|\mathbf{x}_s - \mathbf{x}_r\|},$$

that is to say, using (5)

$$\nabla \bar{u}(\mathbf{x}_g)_i \cdot \mathbf{n}_{i\ell} = \alpha_{gi} \frac{\bar{u}(\mathbf{x}_g) - \bar{u}_i + \bar{r}_{gi}}{\|\mathbf{x}_g - \mathbf{x}_i\|} + \beta_{gi} \frac{\bar{u}(\mathbf{x}_s) - \bar{u}(\mathbf{x}_r) + \bar{r}_{rs}}{\|\mathbf{x}_s - \mathbf{x}_r\|}, \quad (9)$$

$$\nabla \bar{u}(\mathbf{x}_g)_j \cdot \mathbf{n}_{i\ell} = \alpha_{gj} \frac{\bar{u}_j - \bar{u}(\mathbf{x}_g) + \bar{r}_{gj}}{\|\mathbf{x}_j - \mathbf{x}_g\|} + \beta_{gj} \frac{\bar{u}(\mathbf{x}_s) - \bar{u}(\mathbf{x}_r) + \bar{r}_{rs}}{\|\mathbf{x}_s - \mathbf{x}_r\|}, \quad (10)$$

If κ is continuous on a Gauss point \mathbf{x}_g of an edge ℓ we define

$$\kappa_{gi} = \kappa_{gj} = \kappa(\mathbf{x}_g)$$

while if it is not we define

$$\kappa_{gi} = \lim_{\mathbf{x} \in i \rightarrow \mathbf{x}_g} \kappa(\mathbf{x}), \quad \kappa_{gj} = \lim_{\mathbf{x} \in j \rightarrow \mathbf{x}_g} \kappa(\mathbf{x}).$$

Thanks to the continuity of the flux

$$\kappa_{gi} \nabla \bar{u}(\mathbf{x}_g)_i \cdot \mathbf{n}_{i\ell} = \kappa_{gj} \nabla \bar{u}(\mathbf{x}_g)_j \cdot \mathbf{n}_{i\ell},$$

we obtain

$$\begin{aligned} \bar{u}(\mathbf{x}_g) &= \frac{1}{\frac{\kappa_{gi} \alpha_{gi}}{\|\mathbf{x}_g - \mathbf{x}_i\|} + \frac{\kappa_{gj} \alpha_{gj}}{\|\mathbf{x}_j - \mathbf{x}_g\|}} \left(\frac{\kappa_{gj} \alpha_{gj}}{\|\mathbf{x}_j - \mathbf{x}_g\|} (\bar{u}_j + \bar{r}_{gj}) + \frac{\kappa_{gi} \alpha_{gi}}{\|\mathbf{x}_g - \mathbf{x}_i\|} (\bar{u}_i - \bar{r}_{gi}) \right) \\ &\quad + \frac{\kappa_{gj} \beta_{gj}}{\|\mathbf{x}_s - \mathbf{x}_r\|} (\bar{u}(\mathbf{x}_s) - \bar{u}(\mathbf{x}_r) + \bar{r}_{rs}) - \frac{\kappa_{gi} \beta_{gi}}{\|\mathbf{x}_s - \mathbf{x}_r\|} (\bar{u}(\mathbf{x}_s) - \bar{u}(\mathbf{x}_r) + \bar{r}_{rs}). \end{aligned}$$

Inserting this value into (9) or (10) results in

$$\begin{aligned}
\kappa_{gi} \nabla \bar{u}(\mathbf{x}_g)_i \cdot \mathbf{n}_{i\ell} &= \kappa_{gj} \nabla \bar{u}(\mathbf{x}_g)_j \cdot \mathbf{n}_{i\ell} = \left(\frac{\kappa_{gi} \kappa_{gj} \alpha_{gi} \alpha_{gj}}{\|\mathbf{x}_j - \mathbf{x}_g\| \kappa_{gi} \alpha_{gi} + \|\mathbf{x}_g - \mathbf{x}_i\| \kappa_{gj} \alpha_{gj}} \right) (\bar{u}_j - \bar{u}_i + \bar{r}_{gj} + \bar{r}_{gi}) \\
&+ \left(\frac{\kappa_{gi} \kappa_{gj} \alpha_{gi} \beta_{gj} \|\mathbf{x}_j - \mathbf{x}_g\|}{\|\mathbf{x}_s - \mathbf{x}_r\| (\|\mathbf{x}_j - \mathbf{x}_g\| \kappa_{gi} \alpha_{gi} + \|\mathbf{x}_g - \mathbf{x}_i\| \kappa_{gj} \alpha_{gj})} \right) (\bar{u}(\mathbf{x}_s) - \bar{u}(\mathbf{x}_r) + \bar{r}_{rs}) \\
&+ \left(\frac{\kappa_{gi} \kappa_{gj} \alpha_{gj} \beta_{gi} \|\mathbf{x}_g - \mathbf{x}_i\|}{\|\mathbf{x}_s - \mathbf{x}_r\| (\|\mathbf{x}_j - \mathbf{x}_g\| \kappa_{gi} \alpha_{gi} + \|\mathbf{x}_g - \mathbf{x}_i\| \kappa_{gj} \alpha_{gj})} \right) (\bar{u}(\mathbf{x}_s) - \bar{u}(\mathbf{x}_r) + \bar{r}_{rs}).
\end{aligned}$$

Let us assume that we have at our disposal an approximation $\mathbf{u} = (u_i)_{1 \leq i \leq n}$ of $\bar{\mathbf{u}} = (\bar{u}_i)_{1 \leq i \leq n}$. From \mathbf{u} we can find a high-order polynomial approximation $P_i(\mathbf{x})$ of \bar{u} in each cell i while respecting the discontinuity lines of the diffusion coefficient κ (see Section 3.3). So, the numerical flux $\mathcal{F}_\ell(\mathbf{u})$ is defined by

$$\begin{aligned}
\mathcal{F}_\ell(\mathbf{u}) &= |\ell| \sum_{g \in \ell} \omega_g \left[\left(\frac{\kappa_{gi} \kappa_{gj} \alpha_{gi} \alpha_{gj}}{\|\mathbf{x}_j - \mathbf{x}_g\| \kappa_{gi} \alpha_{gi} + \|\mathbf{x}_g - \mathbf{x}_i\| \kappa_{gj} \alpha_{gj}} \right) (u_j - u_i + r_{gj}(\mathbf{u}) + r_{gi}(\mathbf{u})) \right. \\
&+ \left(\frac{\kappa_{gi} \kappa_{gj} \alpha_{gi} \beta_{gj} \|\mathbf{x}_j - \mathbf{x}_g\|}{\|\mathbf{x}_s - \mathbf{x}_r\| (\|\mathbf{x}_j - \mathbf{x}_g\| \kappa_{gi} \alpha_{gi} + \|\mathbf{x}_g - \mathbf{x}_i\| \kappa_{gj} \alpha_{gj})} \right) (P_j(\mathbf{x}_s) - P_j(\mathbf{x}_r) + s_{gj}(\mathbf{u})) \\
&\left. + \left(\frac{\kappa_{gi} \kappa_{gj} \alpha_{gj} \beta_{gi} \|\mathbf{x}_g - \mathbf{x}_i\|}{\|\mathbf{x}_s - \mathbf{x}_r\| (\|\mathbf{x}_j - \mathbf{x}_g\| \kappa_{gi} \alpha_{gi} + \|\mathbf{x}_g - \mathbf{x}_i\| \kappa_{gj} \alpha_{gj})} \right) (P_i(\mathbf{x}_s) - P_i(\mathbf{x}_r) + s_{gi}(\mathbf{u})) \right]
\end{aligned}$$

with

$$\left\{ \begin{aligned}
r_{gi}(\mathbf{u}) &= \frac{1}{V_i} \sum_{p=2}^k \sum_{q=0}^p N_q^p \frac{\partial^p P_i}{\partial x^q \partial y^{p-q}}(\mathbf{x}_g) \int_i (x - x_g)^q (y - y_g)^{p-q} dx, \\
r_{gj}(\mathbf{u}) &= -\frac{1}{V_j} \sum_{p=2}^k \sum_{q=0}^p N_q^p \frac{\partial^p P_j}{\partial x^q \partial y^{p-q}}(\mathbf{x}_g) \int_j (x - x_g)^q (y - y_g)^{p-q} dx, \\
s_{gi}(\mathbf{u}) &= -\sum_{p=2}^k \sum_{q=0}^p N_q^p \frac{\partial^p P_i}{\partial x^q \partial y^{p-q}}(\mathbf{x}_g) ((x_s - x_g)^q (y_s - y_g)^{p-q} - (x_r - x_g)^q (y_r - y_g)^{p-q}), \\
s_{gj}(\mathbf{u}) &= -\sum_{p=2}^k \sum_{q=0}^p N_q^p \frac{\partial^p P_j}{\partial x^q \partial y^{p-q}}(\mathbf{x}_g) ((x_s - x_g)^q (y_s - y_g)^{p-q} - (x_r - x_g)^q (y_r - y_g)^{p-q}).
\end{aligned} \right. \quad (11)$$

Finally we obtain in a more compact form the following approximation of the flux through the edge ℓ

$$\mathcal{F}_\ell(\mathbf{u}) = \gamma_\ell (u_j - u_i) + r_\ell(\mathbf{u}) \quad (12)$$

with

$$\left\{ \begin{aligned}
\gamma_\ell &= |\ell| \sum_{g \in \ell} \omega_g \left(\frac{\kappa_{gi} \kappa_{gj} \alpha_{gi} \alpha_{gj}}{\|\mathbf{x}_j - \mathbf{x}_g\| \kappa_{gi} \alpha_{gi} + \|\mathbf{x}_g - \mathbf{x}_i\| \kappa_{gj} \alpha_{gj}} \right) \geq 0, \\
r_\ell(\mathbf{u}) &= |\ell| \sum_{g \in \ell} \omega_g \left[\left(\frac{\kappa_{gi} \kappa_{gj} \alpha_{gi} \alpha_{gj}}{\|\mathbf{x}_j - \mathbf{x}_g\| \kappa_{gi} \alpha_{gi} + \|\mathbf{x}_g - \mathbf{x}_i\| \kappa_{gj} \alpha_{gj}} \right) (r_{gi}(\mathbf{u}) + r_{gj}(\mathbf{u})) \right. \\
&+ \left(\frac{\kappa_{gi} \kappa_{gj} \alpha_{gj} \beta_{gi} \|\mathbf{x}_g - \mathbf{x}_i\|}{\|\mathbf{x}_s - \mathbf{x}_r\| (\|\mathbf{x}_j - \mathbf{x}_g\| \kappa_{gi} \alpha_{gi} + \|\mathbf{x}_g - \mathbf{x}_i\| \kappa_{gj} \alpha_{gj})} \right) (P_i(\mathbf{x}_s) - P_i(\mathbf{x}_r) + s_{gi}(\mathbf{u})) \\
&\left. + \left(\frac{\kappa_{gi} \kappa_{gj} \alpha_{gi} \beta_{gj} \|\mathbf{x}_j - \mathbf{x}_g\|}{\|\mathbf{x}_s - \mathbf{x}_r\| (\|\mathbf{x}_j - \mathbf{x}_g\| \kappa_{gi} \alpha_{gi} + \|\mathbf{x}_g - \mathbf{x}_i\| \kappa_{gj} \alpha_{gj})} \right) (P_j(\mathbf{x}_s) - P_j(\mathbf{x}_r) + s_{gj}(\mathbf{u})) \right].
\end{aligned} \right.$$

3.2 Approximation of the boundary fluxes

In this section we use the boundary conditions to estimate the boundary fluxes.

3.2.1 Neumann boundary condition

Integrating the Neumann boundary condition on an edge $\ell \subset \Gamma_N$, we have

$$\int_\ell \kappa \nabla \bar{u} \cdot \mathbf{n} = \int_\ell g_N,$$

that is to say

$$\bar{\mathcal{F}}_\ell = |\ell| \sum_{g \in \ell} \omega_g g_N(\mathbf{x}_g) + \mathcal{O}(h^k),$$

we thus impose this equation on the numerical flux

$$\mathcal{F}_\ell(\mathbf{u}) = |\ell| \sum_{g \in \ell} \omega_g g_N(\mathbf{x}_g).$$

3.2.2 Dirichlet boundary condition

Taking into account the Dirichlet boundary condition $\bar{u}(\mathbf{x}_g) = g_D(\mathbf{x}_g)$ in (9) we have, for $g \in \ell \subset \Gamma_D$,

$$\nabla \bar{u}(\mathbf{x}_g) \cdot \mathbf{n}_{i\ell} = \alpha_{gi} \frac{g_D(\mathbf{x}_g) - \bar{u}_i + \bar{r}_{gi}}{\|\mathbf{x}_g - \mathbf{x}_i\|} + \beta_{gi} \frac{\bar{u}(\mathbf{x}_s) - \bar{u}(\mathbf{x}_r) + \bar{r}_{rs}}{\|\mathbf{x}_s - \mathbf{x}_r\|}.$$

By mimicking the expression of this exact flux, the numerical one is defined by

$$\mathcal{F}_\ell(\mathbf{u}) = |\ell| \sum_{g \in \ell} \omega_g \kappa_g \left(\frac{\alpha_{gi}}{\|\mathbf{x}_g - \mathbf{x}_i\|} (g_D(\mathbf{x}_g) - u_i + r_{gi}(\mathbf{u})) + \frac{\beta_{gi}}{\|\mathbf{x}_s - \mathbf{x}_r\|} (P_i(\mathbf{x}_s) - P_i(\mathbf{x}_r) + s_{gi}(\mathbf{u})) \right)$$

with $r_{gi}(\mathbf{u})$ and $s_{gi}(\mathbf{u})$ given in (11). In a more compact form we have

$$\mathcal{F}_\ell(\mathbf{u}) = -\gamma_\ell u_i + \sum_{g \in \ell} \left(\frac{\omega_g \kappa_g \alpha_{gi} |\ell|}{\|\mathbf{x}_g - \mathbf{x}_i\|} g_D(\mathbf{x}_g) \right) + r_\ell(\mathbf{u})$$

with

$$\begin{cases} \gamma_\ell = \sum_{g \in \ell} \left(\frac{\omega_g \kappa_g \alpha_{gi} |\ell|}{\|\mathbf{x}_g - \mathbf{x}_i\|} \right) \geq 0, \\ r_\ell(\mathbf{u}) = |\ell| \sum_{g \in \ell} \omega_g \kappa_g \left(\frac{\alpha_{gi}}{\|\mathbf{x}_g - \mathbf{x}_i\|} r_{gi}(\mathbf{u}) + \frac{\beta_{gi}}{\|\mathbf{x}_s - \mathbf{x}_r\|} (P_i(\mathbf{x}_s) - P_i(\mathbf{x}_r) + r_{rs}(\mathbf{u})) \right). \end{cases}$$

3.3 High-order reconstruction by interpolation

For a polynomial of degree k , we have to calculate

$$\frac{(k+1)(k+2)}{2}$$

coefficients, so at least $(k+1)(k+2)$ neighboring cells of the cell are required for stability purpose [17, 23]. When it is possible, the stencil will be centered on the cell, but the closer the cell is to the boundary or the discontinuity of κ , the more the stencil will be shifted in order to not to cross the discontinuity.

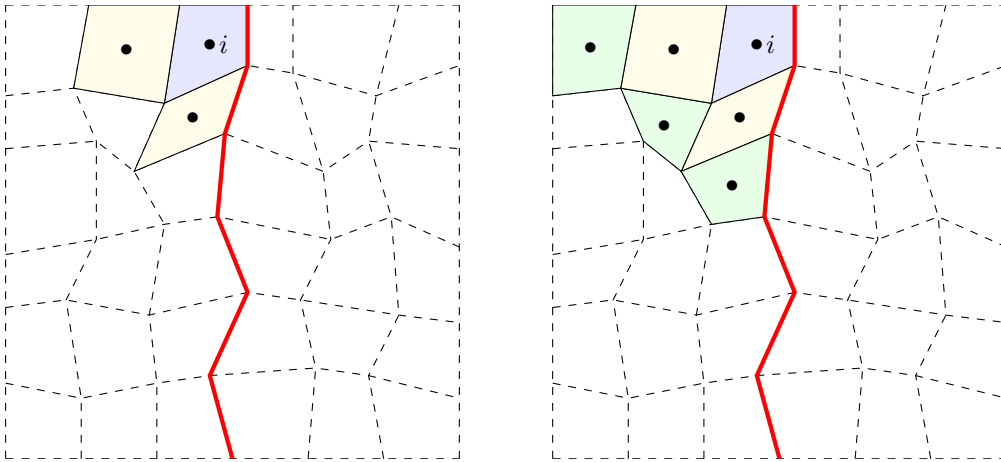


Figure 2: Construction of the stencil for the cell i with a discontinuity (in red)

To be more precise, the construction of the stencil $\mathcal{S}_i = \{0, \dots, p\}$ associated with a cell i is illustrated on Figure 2. For the sake of simplicity, we have assumed that the cells involved in the stencil have been renumbered. First the cell i itself (in blue) is added to the stencil and then we add the cells that share, at least, an edge with the cell i (in yellow). If the number of cells we have already selected is not sufficient (in our case, $(k+1)(k+2)$ cells for a polynomial of order k), we add the cells that have, at least, an edge linked to the cells that we have just been added to the stencil (in green) and so on until we have enough cells. In all the above process, we impose that the stencil does not cross any discontinuity of κ (see Figure 2).

Let u_0, \dots, u_p denote the $p+1$ values of \mathbf{u} used for the calculation, with $p \geq 2$. The polynomial is of the form

$$P(\mathbf{x}) = \sum_{m=0}^k \sum_{n=0}^{k-m} a_{m,n}(\mathbf{u})(x-x_i)^m (y-y_i)^n.$$

The coefficients of the polynomial $P(\mathbf{x})$ are assumed to satisfy

$$\frac{1}{V_j} \int_j P(\mathbf{x}) dx = u_j, \quad \forall j \in \mathcal{S}_i.$$

This leads to the following system

$$\underbrace{\begin{pmatrix} 1 & \frac{1}{V_0} \int_0 (x-x_i) & \frac{1}{V_0} \int_0 (y-y_i) & \dots & \frac{1}{V_0} \int_0 (x-x_i)^k & \frac{1}{V_0} \int_0 (y-y_i)^k \\ \vdots & \vdots & \vdots & \ddots & \vdots & \vdots \\ 1 & \frac{1}{V_p} \int_p (x-x_i) & \frac{1}{V_p} \int_p (y-y_i) & \dots & \frac{1}{V_p} \int_p (x-x_i)^k & \frac{1}{V_p} \int_p (y-y_i)^k \end{pmatrix}}_{=: \mathbf{M}} \underbrace{\begin{pmatrix} a_{0,0} \\ a_{1,0} \\ a_{0,1} \\ \vdots \\ a_{k,0} \\ a_{0,k} \end{pmatrix}}_{=: \mathbf{a}} = \underbrace{\begin{pmatrix} u_0 \\ \vdots \\ u_p \end{pmatrix}}_{=: \mathbf{d}}.$$

Since the matrix \mathbf{M} has more rows than columns we have to use the least square method so that the vector \mathbf{a} is computed as the solution to the linear system: $\mathbf{M}^t \mathbf{M} \mathbf{a} = \mathbf{M}^t \mathbf{d}$. We use the Givens method (see [22] p.206 and following) to solve the least-square problem.

In this process, we do not enforce the continuity of u at the vertices. Indeed, a priori, $P_j(\mathbf{x}_s) \neq P_i(\mathbf{x}_s)$ for $i \neq j$.

4 Monotonicity

A method borrowed from [36, 21, 39, 20] and developed in the framework of 2D diffusion on arbitrary meshes can be used to make the scheme monotonic. The flux (12) can be rewritten as follows

$$\mathcal{F}_\ell(\mathbf{u}) = \gamma_\ell(u_j - u_i) + r_\ell(\mathbf{u})^+ - r_\ell(\mathbf{u})^-$$

with

$$r_\ell(\mathbf{u})^+ = \frac{|r_\ell(\mathbf{u})| + r_\ell(\mathbf{u})}{2} \geq 0 \quad \text{and} \quad r_\ell(\mathbf{u})^- = \frac{|r_\ell(\mathbf{u})| - r_\ell(\mathbf{u})}{2} \geq 0.$$

Let us assume that $\mathbf{u} > \mathbf{0}$, the flux then reads as

$$\mathcal{F}_\ell(\mathbf{u}) = \left(\gamma_\ell + \frac{r_\ell(\mathbf{u})^+}{u_j} \right) u_j - \left(\gamma_\ell + \frac{r_\ell(\mathbf{u})^-}{u_i} \right) u_i$$

and the coefficients $\left(\gamma_\ell + \frac{r_\ell(\mathbf{u})^+}{u_j} \right)$ and $\left(\gamma_\ell + \frac{r_\ell(\mathbf{u})^-}{u_i} \right)$ are positive. We end up with a two-point flux, which is very favorable for the resolution of the system. However note that this system is non-symmetric and non-linear since its coefficients depend on \mathbf{u} .

4.1 Matrix form

The scheme reads as

$$-\sum_{\ell \in \mathcal{I}} \mathcal{F}_\ell(\mathbf{u}) + \lambda_i V_i u_i = V_i f_i. \quad (13)$$

Consider a mesh the cells of which are numbered from 1 to n . Denoting

$$\mathbf{u} = (u_i)_{1 \leq i \leq n}, \quad \mathbf{b} = (b_i)_{1 \leq i \leq n}, \quad \mathbf{A} = (A_{ij})_{1 \leq i, j \leq n},$$

we can write (13) as the matrix-vector product

$$\mathbf{A}(\mathbf{u})\mathbf{u} = \mathbf{b}, \tag{14}$$

with

$$\begin{cases} A_{ii}(\mathbf{u}) = \sum_{\ell \in i, \ell \notin \Gamma_N} \left(\gamma_\ell + \frac{r_\ell(\mathbf{u})^-}{u_i} \right) + V_i \lambda_i, \\ A_{ij}(\mathbf{u}) = - \sum_{\ell \in i \cap j} \left(\gamma_\ell + \frac{r_\ell(\mathbf{u})^+}{u_j} \right) & i \neq j \end{cases} \tag{15}$$

and

$$\mathbf{b}_i = V_i f_i + \sum_{\ell \in i, \ell \in \Gamma_D} \left(r_\ell(\mathbf{u})^+ + \sum_{g \in \ell} \left(\frac{\omega_g \kappa_g \alpha_{gi} |\ell|}{\|\mathbf{x}_g - \mathbf{x}_i\|} \right) g_D(\mathbf{x}_g) \right) + \sum_{\ell \in i, \ell \in \Gamma_N} |\ell| \sum_{g \in \ell} \omega_g g_N(\mathbf{x}_g). \tag{16}$$

Remark 4.1. Assuming that $f \geq 0$ and $g \geq 0$, all the components of the right hand side \mathbf{b} are non-negative. Assuming moreover that f and g are not both identically zero, then at least one component of \mathbf{b} is positive.

4.2 Picard iteration method

In order to solve (14) we use a Picard iteration method. We start with an initial guess $\mathbf{u}^0 > 0$, compute the matrix $\mathbf{A}(\mathbf{u}^0)$ and solve $\mathbf{A}(\mathbf{u}^0)\mathbf{u}^1 = \mathbf{b}$. Repeating this process, we build a sequence (\mathbf{u}^ν) that, if it converges to a positive vector, tends to a solution of the scheme. We stop the algorithm when the difference $\mathbf{u}^{\nu+1} - \mathbf{u}^\nu$ between two successive iterates is small enough. To summarize, the following algorithm is used

$$\begin{aligned} \nu &= 0 \\ A(\mathbf{u}^0)\mathbf{u}^1 &= \mathbf{b} \\ \text{While } \frac{\|\mathbf{u}^{\nu+1} - \mathbf{u}^\nu\|_2}{\|\mathbf{u}^\nu\|_2} &> \mu \\ A(\mathbf{u}^\nu)\mathbf{u}^{\nu+1} &= \mathbf{b} \\ \nu &= \nu + 1. \end{aligned} \tag{17}$$

Unfortunately, we are unable to prove that the above algorithm converges. Nevertheless, we prove in Section 5.3 below that the scheme is well defined at each iteration of the algorithm, as soon as the initial guess \mathbf{u}^0 is positive.

5 Properties

5.1 Conservation

By construction note that the scheme is conservative.

Proposition 5.1. Assume that $\mathbf{u} > \mathbf{0}$ and consider homogeneous Neumann boundary conditions, then the scheme defined by (13) is conservative, that is to say

$$\sum_{i=1}^n V_i \lambda_i u_i = \sum_{i=1}^n V_i f_i.$$

Indeed it satisfies the equality

$$\sum_{i=1}^n \left(- \sum_{\ell \in i} \mathcal{F}_\ell(\mathbf{u}) \right) = 0.$$

5.2 Monotonicity

Consider the definition of an M-matrix (see for instance [29])

Definition 5.2. An $n \times n$ matrix \mathbf{A} that can be expressed in the form $\mathbf{A} = s\mathbf{I} - \mathbf{B}$, where $\mathbf{B} = (b_{ij})_{1 \leq i, j \leq n}$ with $b_{ij} \geq 0$, $1 \leq i, j \leq n$, and $s \geq \rho(\mathbf{B})$, the maximum of the moduli of the eigenvalues of \mathbf{B} , is called an M-matrix.

We use the following lemma

Lemma 5.3. A matrix $\mathbf{A} = (A_{ij})_{1 \leq i, j \leq n}$ is an M-matrix if it satisfies the following inequalities

$$\forall i \neq j, \quad A_{ij} \leq 0, \quad \text{and} \quad \forall i, \quad \sum_{j=1}^n A_{ij} \geq 0.$$

Moreover, if the last inequality is strict, we say that \mathbf{A} is a strict M-matrix.

Proposition 5.4. Assume that $\mathbf{u} > \mathbf{0}$. Then the matrix \mathbf{A} defined by (15) is such that \mathbf{A}^t is a strict M-matrix.

Proof. The matrix \mathbf{A} satisfies

$$\forall i \neq j, \quad A_{ij} \leq 0 \quad \text{and} \quad \forall j, \quad \sum_{i=1}^n A_{ij} > 0.$$

Indeed we have, for all j

$$\sum_{i=1}^n A_{ij} = \sum_{i=1}^n \left(\sum_{\ell \in i, \ell \notin \Gamma_N} \left(\gamma_\ell + \frac{r_\ell(\mathbf{u})^-}{u_i} \right) - \sum_{\ell \in i \cap j} \left(\gamma_\ell + \frac{r_\ell(\mathbf{u})^+}{u_j} \right) \right) + \lambda_j V_j.$$

Thanks to Proposition 5.1, only the boundary terms and the mass term remain, for all j

$$\sum_{i=1}^n A_{ij} = \sum_{i=1}^n \sum_{\ell \in (i \cap \Gamma_D)} \left(\gamma_\ell + \frac{r_\ell(\mathbf{u})^-}{u_i} \right) + \lambda_j V_j > 0.$$

□

Theorem 5.5. Assume that $f > 0$ and $g > 0$. Let \mathbf{A} and \mathbf{b} be defined by (15)-(16). Then $\mathbf{A}^{-1}\mathbf{b} = \mathbf{u} \geq \mathbf{0}$.

Proof. As \mathbf{A}^t is a strict M-matrix \mathbf{A} is invertible and its inverse has only non-negative entries (see for example [33], Corollary 3.20). In view of Remark 4.1, the right hand side is non-negative, hence $\mathbf{u} = \mathbf{A}^{-1}\mathbf{b} \geq \mathbf{0}$. □

Remark 5.6. The scheme preserves positivity if the inversion of the linear system is exact. The above proof assumes that the matrix M^{-1} is calculated exactly. Obviously, in practice, this is not the case. In the tests we have carried out, the error is small enough not to affect the calculations. However, in rare cases, the inversion of the matrix led to a solution with negative components, causing the calculation to stop. This error can be reduced by working on the condition number of the matrix or on methods for solving linear systems, which is a perspective.

5.3 Well-posedness of the Picard iteration method

Proposition 5.7. Assume that $f \geq 0$, $g \geq 0$, and either $\|f\|_{L^2(\Omega)} > 0$ or $\|g\|_{L^2(\partial\Omega)} > 0$. Assume moreover that $\mathbf{u}^0 > \mathbf{0}$. Then, the algorithm (17) defines a sequence $(\mathbf{u}^\nu)_{\nu \geq 0}$ such, that for all ν , $\mathbf{u}^\nu > \mathbf{0}$.

To prove this property, we need to introduce the concept of irreducible matrix: see [33, Definition 1.15].

Definition 5.8. An $n \times n$ matrix \mathbf{A} is **reducible** if there exists an $n \times n$ permutation matrix \mathbf{P} such that

$$\mathbf{P}\mathbf{A}\mathbf{P}^t = \begin{bmatrix} \mathbf{A}_{11} & \mathbf{A}_{12} \\ \mathbf{0} & \mathbf{A}_{22} \end{bmatrix},$$

where \mathbf{A}_{11} , \mathbf{A}_{12} , \mathbf{A}_{22} are respectively $r \times r$, $r \times (n-r)$ and $(n-r) \times (n-r)$ sub-matrices with $1 \leq r < n$. If no such permutation matrix exists, then \mathbf{A} is **irreducible**.

The matrix \mathbf{A} defined by (15) is irreducible thanks to the following Lemma (see [33, Theorem 1.17]).

Lemma 5.9. To any $n \times n$ matrix \mathbf{A} we associate the graph of nodes $1, 2, \dots, n$ and of directed edges connecting \mathbf{x}_i to \mathbf{x}_j if $A_{ij} \neq 0$. Then \mathbf{A} is irreducible if and only if for any pair $i \neq j$ there exists a chain of edges that allows to go from \mathbf{x}_i to \mathbf{x}_j ,

$$A_{i,k_1} \neq 0 \rightarrow A_{k_1,k_2} \neq 0 \rightarrow \dots \rightarrow A_{k_m,j} \neq 0.$$

With these definitions we can make use of the following theorem (see [33], Corollary 3.20).

Theorem 5.10. *If \mathbf{A} is an irreducible strict M -matrix, then it is invertible and, for all i, j ($1 \leq i, j \leq n$), $(\mathbf{A}^{-1})_{ij} > 0$.*

We are now in position to prove Proposition 5.7.

Proof of Proposition 5.7. We argue by induction on the index ν . We assume that $\mathbf{u}^\nu > \mathbf{0}$. Hence $(\mathbf{A}(\mathbf{u}^\nu))^t$ is a strict M -matrix (see Proposition 5.4). It is easy to check that $(\mathbf{A}(\mathbf{u}^\nu))^t$ is also irreducible. Thus, applying Theorem 5.10, $(\mathbf{A}(\mathbf{u}^\nu))^t$ is invertible and all the entries of $(\mathbf{A}(\mathbf{u}^\nu))^{-t}$ are positive. Consequently, all the entries of $(\mathbf{A}(\mathbf{u}^\nu))^{-1}$ are positive. Using Remark 4.1, we know that all components of \mathbf{b} are non-negative. Moreover, because of the assumption that either $\|f\|_{L^2(\Omega)} > 0$ or $\|g\|_{L^2(\partial\Omega)} > 0$, at least one component of \mathbf{b} is positive. We thus have, for all i ($1 \leq i \leq n$)

$$u_i^{\nu+1} = \sum_{j=1}^n (\mathbf{A}(\mathbf{u}^\nu))_{ij}^{-1} b_j > 0,$$

since all terms of this sum are non-negative, with one at least that does not vanish. \square

Proposition 5.7 shows that the condition $\mathbf{u}^\nu > \mathbf{0}$ remains satisfied during the Picard iteration method, which allows to define $\mathbf{A}(\mathbf{u}^\nu)$ for all $\nu \geq 0$.

6 Numerical experiments

Given $\Omega =]0, 1[^2$, κ a diffusion coefficient and g a function defined on $\partial\Omega$, consider Problem (1) with $\lambda = 0$ and $\Gamma_N = \emptyset$

$$\begin{cases} -\nabla \cdot (\kappa \nabla \bar{u}) = f & \text{in } \Omega, \\ \bar{u} = g & \text{on } \partial\Omega. \end{cases} \quad (18)$$

In addition to Cartesian meshes we will use the two following types of meshes (see Figure 3):

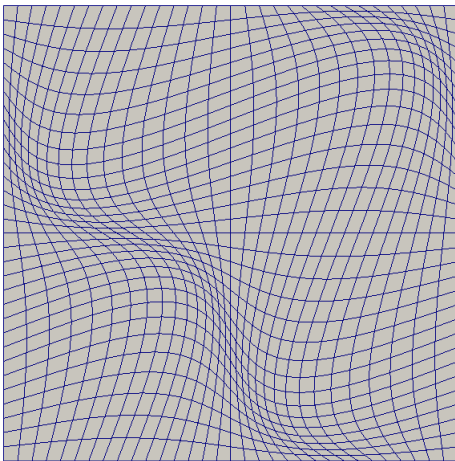
1. deformed meshes, the deformation of which from the Cartesian mesh is given by

$$(x, y) \rightarrow (x + 0.1 \sin(2\pi x) \sin(2\pi y), y + 0.1 \sin(2\pi x) \sin(2\pi y)),$$

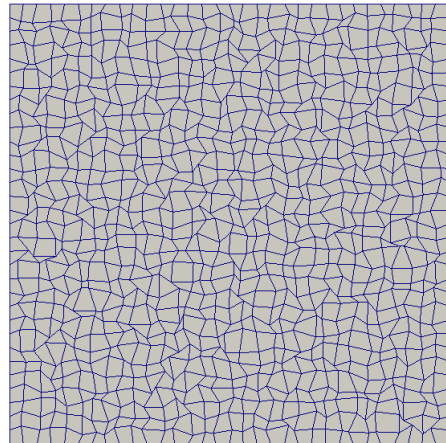
2. randomly deformed meshes, the deformation of which from the unit Cartesian mesh with cells of size Δx is given by

$$(x, y) \rightarrow 0.1(x, y) + 0.9(x + 0.45a\Delta x, y + 0.45b\Delta x),$$

where a, b are random numbers distributed according to the uniform law on $[-1, 1]$.



(a) A deformed mesh



(b) A randomly deformed mesh

Figure 3: Examples of deformed meshes.

The L^2 -error on the solution and the L^2 -error on the fluxes used in the following tests are respectively given by

$$\frac{\|\mathbf{u} - \bar{\mathbf{u}}\|_2}{\|\bar{\mathbf{u}}\|_2}, \frac{\left(\sum_{\ell} \left(\mathcal{F}_{\ell}(\mathbf{u}) - |\ell| \sum_{g \in \ell} \omega_g \kappa_g \nabla \bar{u}(\mathbf{x}_g) \cdot \mathbf{n}_{i\ell} \right)^2 \right)^{1/2}}{\left(\sum_{\ell} \left(|\ell| \sum_{g \in \ell} \omega_g \kappa_g \nabla \bar{u}(\mathbf{x}_g) \cdot \mathbf{n}_{i\ell} \right)^2 \right)^{1/2}},$$

We also use the H^1 semi-norm error defined by

$$\frac{\|\nabla_h \mathbf{u} - \nabla \bar{u}\|_2}{\|\nabla \bar{u}\|_2},$$

where

$$\|\nabla \bar{u}\|_2 = \left(\sum_i V_i \|\nabla \bar{u}(\mathbf{x}_i)\|^2 \right)^{1/2}, \quad \|\nabla_h \mathbf{u} - \nabla \bar{u}\|_2 = \left(\sum_i V_i \|\nabla P_i(\mathbf{x}_i) - \nabla \bar{u}(\mathbf{x}_i)\|^2 \right)^{1/2},$$

P_i being the polynomial obtained by reconstruction with the approximated values of the solution \mathbf{u} .

For all the tests, the stopping criterion μ and the initial guess \mathbf{u}^0 of the fixed-point algorithm (17) are $\mu = 10^{-12}$ and $u_i^0 = 1, \forall i$. We use the linear solver GMRES with the preconditioner ILU (see [28], Chapter 7.4) with the convergence criterion is 10^{-14} .

6.1 Numerical accuracy assessment

In this section we present numerical results for diffusion problems of type (18) with analytical solutions. The first (resp. second) case involves a discontinuous (resp. anisotropic) diffusion coefficient. Numerical convergence rates are evaluated using the L^2 norm of the solution as well the L^2 norm of the fluxes and the H^1 semi-norm. We perform a convergence study for these problems with a sequence of successively refined deformed meshes as that shown in Figure 3a. For the sake of brevity we present only the results on this type of mesh. We obtain similar results on randomly deformed meshes as that shown on Figure 3b. We will also skip the case of continuous scalar diffusion coefficient, as it is simpler than the discontinuous and anisotropic cases.

6.1.1 Discontinuous diffusion coefficient

Recall that we have assumed the possible discontinuities of the diffusion coefficient κ coincide with edges of the mesh. Given

$$\kappa(\mathbf{x}) = \begin{cases} 1 & \text{if } x \leq \frac{1}{2} \\ 2 & \text{if } x > \frac{1}{2} \end{cases}, \quad f(\mathbf{x}) = 2\pi^2 \cos(\pi x) \cos(\pi y) + 20, \quad g(\mathbf{x}) = 0,$$

the function

$$\bar{u}(\mathbf{x}) = \begin{cases} \cos(\pi x) \cos(\pi y) - 10x^2 + 12 & \text{if } x \leq \frac{1}{2}, \\ \frac{1}{2} \cos(\pi x) \cos(\pi y) - 5x^2 + \frac{43}{4} & \text{if } x > \frac{1}{2}, \end{cases}$$

is solution to (18). Results are summarized in Figure 4 which shows that all schemes are k -th-order accurate in the L^2 norm of the solution as well the L^2 norm of the fluxes and the H^1 semi-norm. We can note that there is a superconvergence for odd orders.

We see that, even if $\nabla \bar{u}$ is discontinuous in this problem, we are able to achieve an arbitrary order of accuracy. The by point for this is to design a stencil that do not cross discontinuities of κ , as explained in Section 3.3.

6.1.2 Anisotropic diffusion coefficient

Given

$$\kappa(\mathbf{x}) = \begin{pmatrix} 1 & 0 \\ 0 & 2 \end{pmatrix}, \quad f(\mathbf{x}) = 3\pi^2 \sin(\pi x) \sin(\pi y), \quad g(\mathbf{x}) = 0,$$

the function $\bar{u}(\mathbf{x}) = \sin(\pi x) \sin(\pi y)$ is solution to (18). Results are summarized in Figure 5 which shows that all schemes are k -th-order accurate in the L^2 norm, the L^2 norm of the fluxes and the H^1 semi-norm. We can note that there is

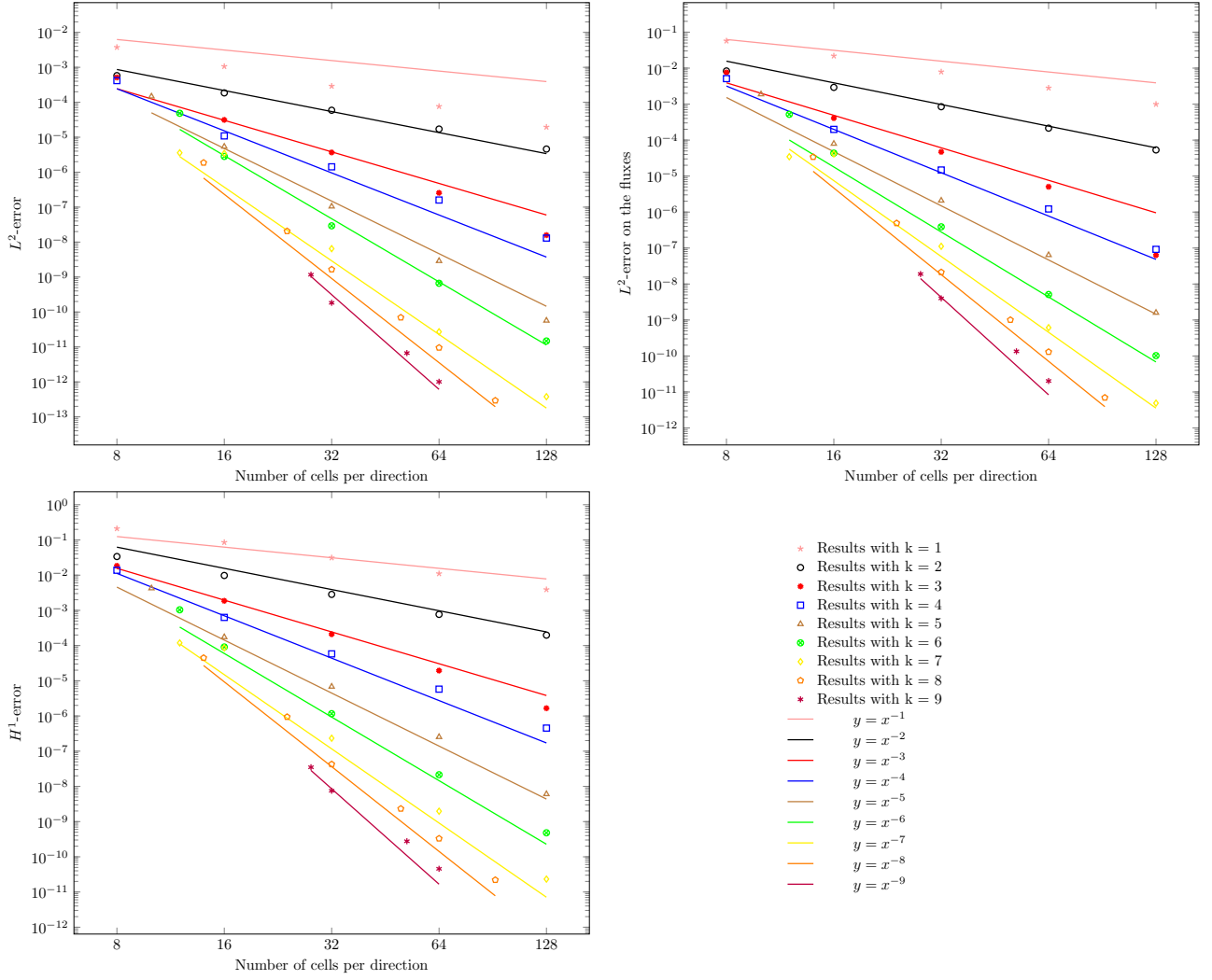


Figure 4: L^2 -error on the solution (top left), L^2 -error on the fluxes (top right) and H^1 semi-norm error (bottom left) for problem of Section 6.1.1.

a superconvergence for odd orders. Of course, similar results have been obtained for a scalar-valued diffusion coefficient κ .

Scheme	Number of cells per direction	Number of iterations	Execution time (ratio)
Order 1	168	172	1
Order 2	212	180	2.33
Order 3	31	132	0.10
Order 4	31	120	0.20
Order 5	19	103	0.20
Order 6	14	124	0.26
Order 7	16	143	1.08
Order 8	10	154	0.78

Table 1: Minimum number of cells to reach a precision on the L^2 -error of 10^{-5} with the time of execution and the number of iterations of the fixed point algorithm for order 1 to 8 for problem of Section 6.1.2.

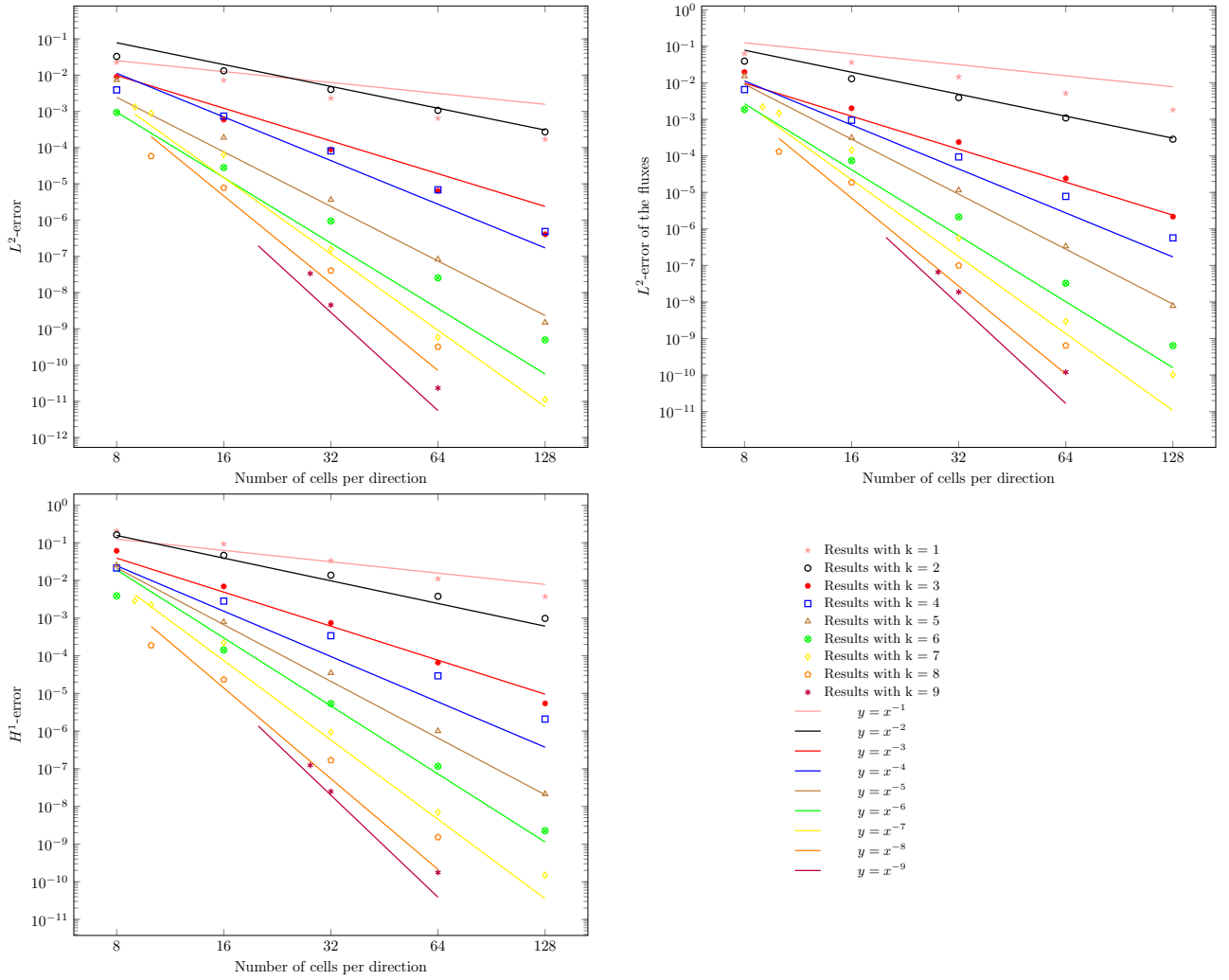


Figure 5: L^2 -error on the solution (top left), L^2 -error on the fluxes (top right) and H^1 semi-norm error (bottom left) for problem of Section 6.1.2.

Scheme	Number of cells per direction	Number of iterations	Execution time (ratio)
Order 3	323	135	1
Order 4	343	135	2.49
Order 5	93	122	0.56
Order 6	76	134	0.73
Order 7	46	90	0.52
Order 8	40	76	0.62
Order 9	30	75	0.75

Table 2: Minimum number of cells to reach a precision on the L^2 -error of 10^{-9} with the time of execution and the number of iterations of the fixed point algorithm for order 3 to 9 for problem of Section 6.1.2.

Table 1 (resp. Table 2) gives the minimum number of cells per direction required to achieve an accuracy of 10^{-5} (resp. 10^{-9}) on the L^2 -error, with the number of iterations of the fixed point algorithm and the time of execution. As expected, the number of cells needed to achieve the desired precision (first column) is a decreasing function of the order. The second column gives the number of fixed point iterations required to satisfy the stagnation criterion. This number is either constant or decreasing with the order, which is not intuitive and is a good point. The more interesting column

is the last one giving the total computational cost of the method. This computational time is a trade-off between the algorithmic complexity and the precision of the method, which both increase with the order. We notice that, in general, execution time decreases as the order increases. For a large error setpoint value (10^{-5}), the optimal choice of scheme is the third-order one. However, when decreasing the error setpoint value (10^{-9}) higher-order schemes perform better, and the optimal order becomes seven. We anticipate that small values of the error setpoint will favor the highest orders. We obtain speed-ups of factors up to ten in term of computational time to reach the desired precision. We also observed that odd orders perform better than even orders. This confirms what we notice on Figures 4 and 5: a super-convergence is achieved for odd orders. We also observe a somewhat spectral convergence: for a fixed mesh size, the error decreases as k grows.

6.2 Monotonicity assessment

We propose a challenging benchmark borrowed from [38] to compare a non-monotonic scheme, which can give nonpositive solutions (in this case the usual DDFV scheme), with our monotonic high-order scheme which always gives nonnegative solutions. For this test we have used Cartesian meshes.

6.2.1 Tensor-valued coefficient κ and square domain with a square hole

Consider the square domain with a square hole $\Omega =]0, 1[^2 \setminus [\frac{4}{9}, \frac{5}{9}]^2$, $f(\mathbf{x}) = 0$ in Ω and $g(\mathbf{x}) = 0$ (resp. $g(\mathbf{x}) = 2$) on the external (resp. internal) boundary. We choose

$$\kappa = \begin{pmatrix} \cos \theta & \sin \theta \\ -\sin \theta & \cos \theta \end{pmatrix} \begin{pmatrix} 1 & 0 \\ 0 & 10^4 \end{pmatrix} \begin{pmatrix} \cos \theta & -\sin \theta \\ \sin \theta & \cos \theta \end{pmatrix}, \quad \theta = \frac{\pi}{6}.$$

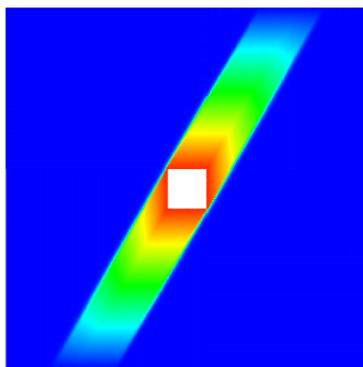


Figure 6: Numerical solution obtained with the DDFV scheme on a highly refined mesh (1310720 cells of size $\Delta x = 1/1152$).

Monotonic scheme	Minimum	Maximum
Order 1	$1.3e - 28$	1.96
Order 2	$1.0e - 21$	1.96
Order 3	$1.7e - 27$	1.98
Order 4	$3.9e - 30$	1.97
Order 5	$1.1e - 27$	1.97
Order 6	$4.3e - 27$	1.98
Order 7	$7.9e - 25$	1.98
Order 8	$5.4e - 21$	1.98

Table 3: Minimum and maximum of the numerical solution to the problem of section 6.2.1 for a Cartesian mesh with 2000 cells of size $\Delta x = 1/45$.

We compare the results obtained with the monotonic high-order schemes on a Cartesian mesh with 2000 cells of size $\Delta x = 1/45$. The stopping criterion of the fixed point algorithm is $\mu = 10^{-12}$, except for order 6 for which $\mu = 10^{-10}$

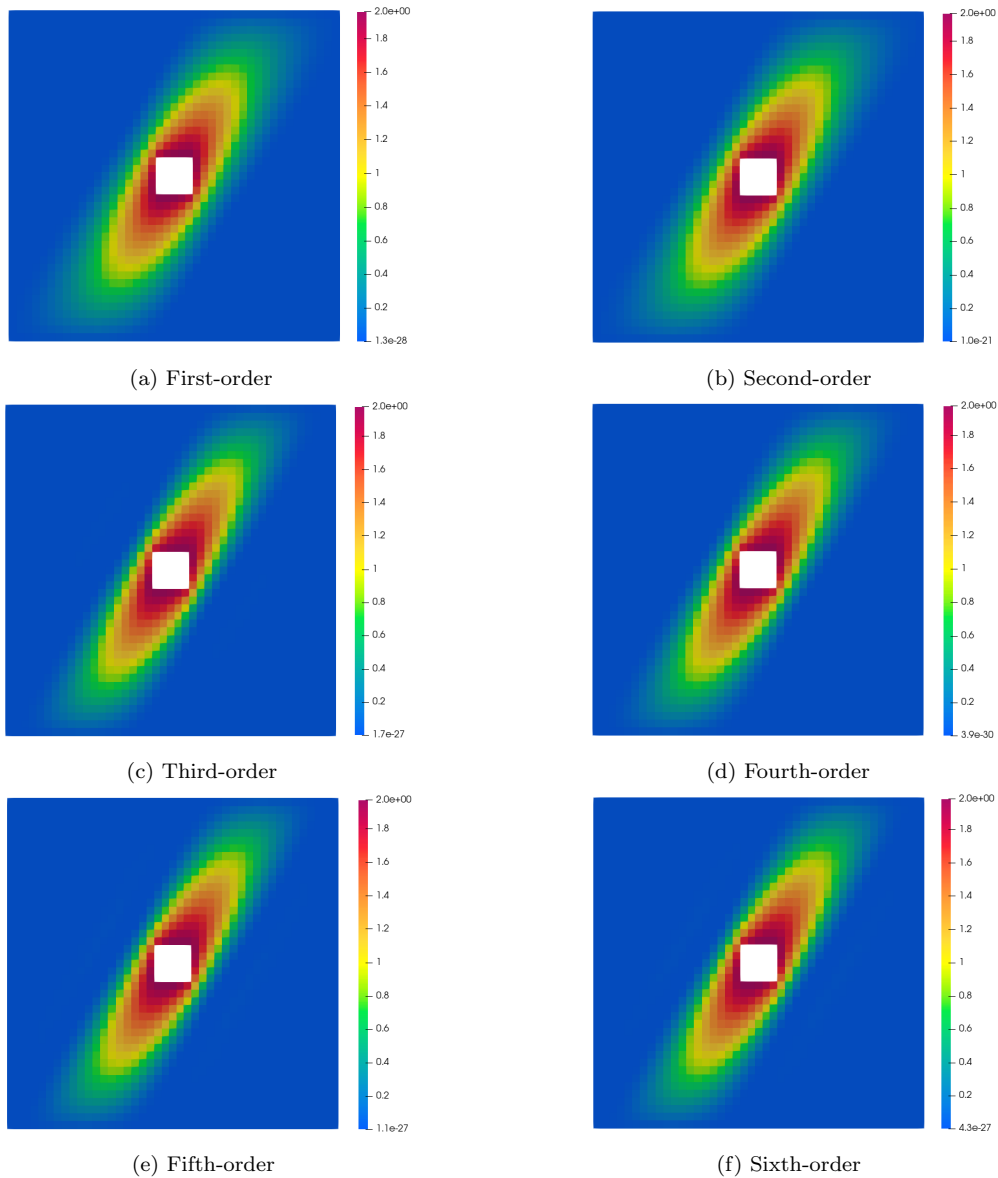


Figure 7: Numerical solutions obtained with monotonic schemes of order 1 to 6 for a Cartesian mesh (2000 cells of size $1/45$).

and for order 7, 8 for which $\mu = 10^{-6}$ to reduce the computing time.

As explained in Remark 5.6, the precision of the inversion of the linear system sometimes leads to negative entries in the solution vector \mathbf{u} . In general, this can be fixed by using the result of a low-order calculation as the initial guess of the high-order calculation. This procedure is also favorable regarding the computation time. It significantly reduces the overall cost of the simulation. However, we encountered one case for which this fix was not sufficient. For the test of order 5, for a Cartesian mesh with 86 cells per direction, we did not manage to run the simulation. We think that this is a severe issue for this kind of methods which is in general not addressed in the papers. In the near future, we intend to work on the linear system inversion.

Even for a highly refined mesh (1310720 squares of size $\Delta x = 1/1152$) the solution obtained with the usual (non-monotonic) DDFV scheme (see Figure 6) has negative values up to -2.11×10^{-3} . On the other hand the high-order solutions obtained with the monotonic scheme remain always positive whatever the order: see Figure 7 and Table 3 which gives the minimum and the maximum of each solution calculated with a Cartesian mesh (2000 cells of size $1/45$), up to order 6. We also observe on Figure 7 that the solution for $k = 3$ is closer to the converged solution (see 6) than the solution for $k = 1$. This is reminiscent of the spectral convergence we pointed out in Section 6.1.

6.2.2 Fokker-Planck type diffusion equation

This benchmark is a simplified version of the one from [25]. Given $\Omega =]-50, 50[^2$, $T = 250$, $\mathbf{v} = (v_x, v_y)$ the velocity variable and $\mathbf{V} = (-20, 20)$ the averaged velocity, we are looking for the distribution function $\bar{u} = \bar{u}(\mathbf{v}, t)$, solution to the simplified Fokker-Planck equation

$$\begin{cases} \frac{\partial \bar{u}}{\partial t} - \nabla_{\mathbf{v}} \cdot (\kappa \nabla_{\mathbf{v}} \bar{u}) = 0 & \text{in } \Omega \times [0, T], \\ \kappa \nabla_{\mathbf{v}} \bar{u} \cdot \mathbf{n} = 0 & \text{on } \partial\Omega \times [0, T], \\ \bar{u}(0) = \bar{u}^0 & \text{in } \Omega, \end{cases} \quad (19)$$

where the diffusion coefficient $\kappa = \kappa(\mathbf{v})$ and the initial condition \bar{u}^0 are given by

$$\kappa(\mathbf{v}) = \mathbf{I} - \frac{1}{\|\mathbf{v}\|^2} \mathbf{v} \otimes \mathbf{v}, \quad \bar{u}^0(\mathbf{v}) = \frac{1}{\pi} \exp(-\|\mathbf{v} - \mathbf{V}\|^2). \quad (20)$$

Note that the full Fokker-Planck equation would read as

$$\frac{\partial \bar{u}}{\partial t} + \nabla_{\mathbf{v}} \cdot (\mathbf{v} \bar{u}) - \nabla_{\mathbf{v}} \cdot (\kappa \nabla_{\mathbf{v}} \bar{u}) = 0.$$

The diffusion coefficient κ defined by (20) is degenerated: it does not satisfy (2), hence the theoretical results of the preceding Sections do not apply to the present case. It follows in particular that the well-posedness of the fixed-point algorithm (see Section 5.3) is no longer ensured. However, \bar{u} should remain positive, and the non-monotonic DDFV scheme produces non-physical negative values. We will see that our monotonic scheme fixes it. This diffusion tensor correspond to a degenerate diffusion problem along the circle of radius $\|\mathbf{v}\|$. The backward Euler scheme is used for time integration.

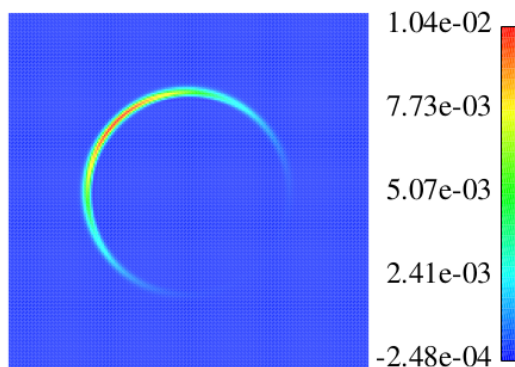


Figure 8: DDFV solution to (19) at time $T = 250$ on the Cartesian mesh of 200×200 cells.

Scheme	Minimum of the solution	Maximum of the solution
DDFV scheme	$-2.48e - 4$	$1.04e - 2$
Monotonic scheme of order 1	$1.5e - 23$	$2.8e - 3$
Monotonic scheme of order 2	$7.5e - 22$	$2.9e - 3$
Monotonic scheme of order 3	$1.1e - 18$	$5.0e - 3$
Monotonic scheme of order 4	$2.5e - 22$	$4.3e - 3$
Monotonic scheme of order 5	$7.8e - 23$	$5.7e - 3$
Monotonic scheme of order 6	$2.3e - 20$	$5.8e - 3$

Table 4: Minimum and maximum of the numerical solution to the problem of section 6.2.2 for the Cartesian mesh with 200 cells per direction.

To limit the calculation time, the stopping criterion of the fixed point algorithm is $\mu = 10^{-5}$. Figure 9 displays the numerical solutions obtained with the Cartesian mesh of 200^2 cells. Table 4 gives the minima and maxima of the DDFV solution and the numerical solution obtained with the monotonic schemes up to order 6. We observe that the minima of the solutions to monotonic schemes always remain non negative, as expected. Compared to the solutions obtained with the DDFV scheme, given by Figures 8 and the solutions obtained by the monotonic DDFV schemes, given in [7], the monotonic arbitrary order schemes are more diffusive (in the radial direction). However, we can note that the higher is the order, the less diffusive (in the radial direction) is the scheme.

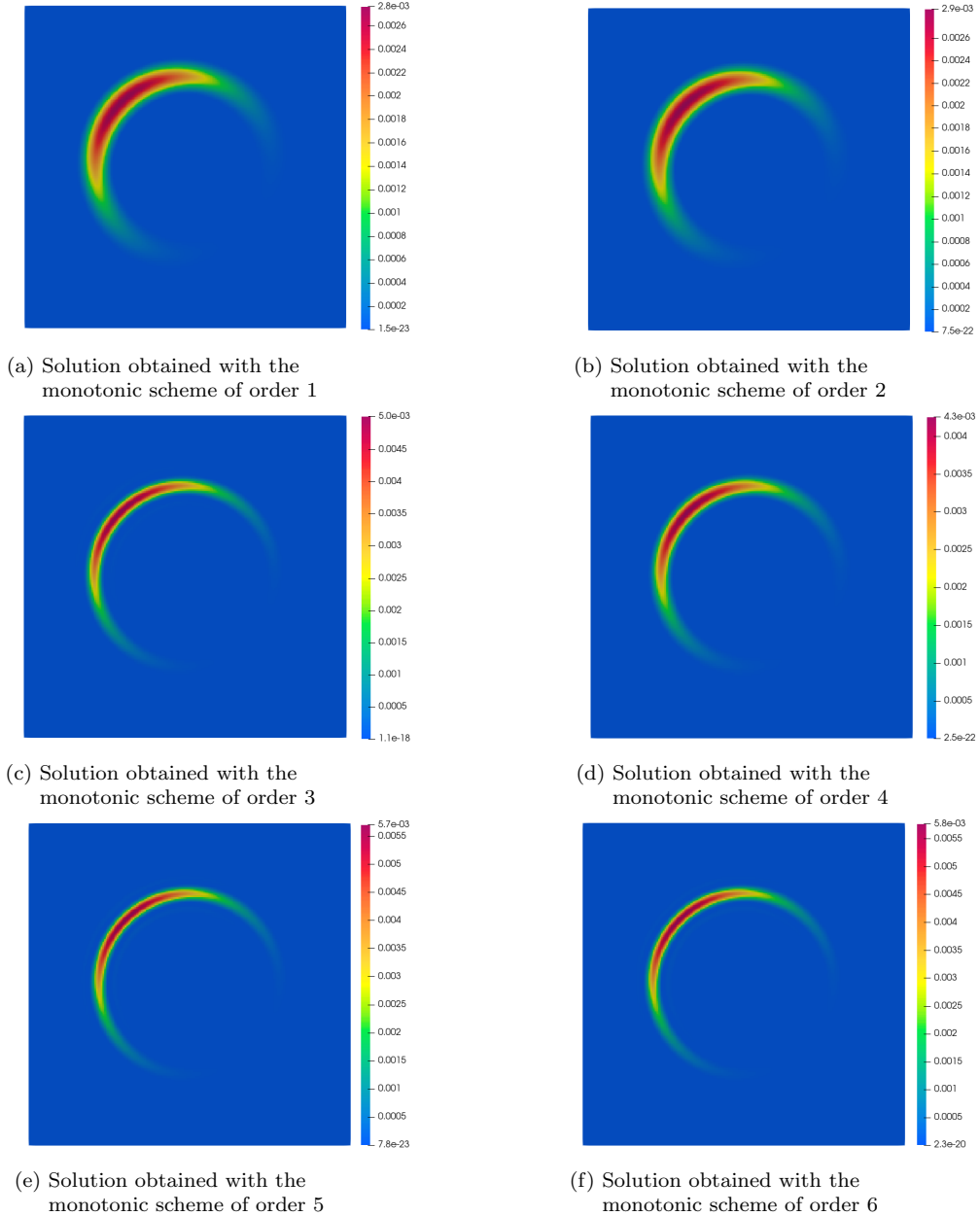


Figure 9: Numerical solutions obtained with monotonic schemes of order 1 to 6 for a Cartesian mesh with 200 cells per direction for problem of Section 6.2.2

7 Concluding remarks

This paper proposes an arbitrary-order monotonic Finite Volume scheme for the elliptic problem (1) on general 2D meshes. The new non-linear method we have detailed here is arbitrary-order convergent even for anisotropic and/or discontinuous diffusion coefficients on deformed meshes. Furthermore it allows to deal with all boundary conditions (Dirichlet, Neumann). This scheme uses a polynomial reconstruction involving values in neighboring cells to evaluate the secondary unknowns at the Gauss quadrature points. We have adapted the non-linear process from [36] to enforce monotonicity. We have assessed numerically both its accuracy and monotonicity.

Numerical performance could be improved. Indeed, the convergence of the fixed-point algorithm is not guaranteed and may be very slow. This is observed in particular in test cases where the classical DDFV scheme gives negative solutions. Techniques for accelerating this fixed point could be explored, such as Anderson acceleration (see [31, 1]) or the ϵ -algorithm (see [9, 8]).

The next step is to extend the method to non-linear diffusion (with a diffusion coefficient depending on the unknown) and to arbitrary order unsteady diffusion, taking inspiration from [18] for example. The extension of the scheme to the three-dimensional case, based on the same ideas, is the subject of ongoing works.

References

- [1] D. G. M. Anderson. Iterative procedures for nonlinear integral equations. *J. ACM*, 12:547–560, 1965.
- [2] G. Barrenechea, V. John, and P. Knobloch. An algebraic flux correction scheme satisfying the discrete maximum principle and linearity preservation on general meshes. *Math. Mod. Meth. Appl. Sci.*, 27(03):525–548, 2017.
- [3] G. Barrenechea, V. John, and P. Knobloch. Finite element methods respecting the discrete maximum principle for convection-diffusion equations, 2023.
- [4] L. Beirão da Veiga, F. Brezzi, L. D. Marini, and A. Russo. Virtual element method for general second-order elliptic problems on polygonal meshes. *Math. Mod. Meth. Appl. Sci.*, 26(04):729–750, 2016.
- [5] E. Bertolazzi and G. Manzini. A second-order maximum principle preserving finite volume method for steady convection-diffusion problems. *SIAM J. Numer. Anal.*, 43(5):2172–2199, 2005.
- [6] X. Blanc, F. Hermeline, E. Labourasse, and J. Patela. Arbitrary-order monotonic finite-volume schemes for 1D elliptic problems. *Comp. Appl. Math.*, 42(4):195, 2023.
- [7] X. Blanc, F. Hermeline, E. Labourasse, and J. Patela. Monotonic diamond and DDFV type finite-volume schemes for 2D elliptic problems. *Commun. Comput. Phys.*, 2023. accepted.
- [8] C. Brezinski. *Accélération de la convergence en analyse numérique*. Lecture notes in mathematics. Springer-Verlag, 1977.
- [9] C. Brezinski. *Algorithmes d'accélération de la convergence: étude numérique*. Collection Langages et algorithmes de l'informatique. Technip, 1978.
- [10] E. Burman and A. Ern. Discrete maximum principle for Galerkin approximations of the Laplace operator on arbitrary meshes. *C. R. Math.*, 338(8):641–646, 2004.
- [11] J.-S. Camier and F. Hermeline. A monotone nonlinear finite volume method for approximating diffusion operators on general meshes. *Int. J. Numer. Meth. Engng*, 107:496–519, 2016.
- [12] C. Cancès and C. Guichard. Numerical analysis of a robust free energy diminishing finite volume scheme for parabolic equations with gradient structure. *Found. Comput. Math.*, 17:1525–1584, 2017.
- [13] G. Carré, S. Del Pino, B. Després, and E. Labourasse. A cell-centered Lagrangian hydrodynamics scheme on general unstructured meshes in arbitrary dimension. *J. Comput. Phys.*, 228(14):5160–5183, 2009.
- [14] P. Ciarlet. *The Finite Element Method for elliptic problems*, volume 40. SIAM, Philadelphia, 2002.
- [15] B. Cockburn, G. E. Karniadakis, and C-W. Shu. *Discontinuous Galerkin methods: theory, computation and applications*, volume 11. Springer Science & Business Media, 2012.
- [16] D. A. Di Pietro and J. Droniou. *The Hybrid High-Order method for polytopal meshes*, volume 19. Springer, 2020.
- [17] M. Dumbser, W. Boscheri, M. Semplice, and G. Russo. Central weighted eno schemes for hyperbolic conservation laws on fixed and moving unstructured meshes. *SIAM J. Sci. Comput.*, 39(6):A2564–A2591, 2017.
- [18] A. Ern and J.-L. Guermond. Invariant-domain preserving high-order time stepping: II. IMEX schemes. *hal-03703035*, v1, 2022.
- [19] L. Evans. Application of nonlinear semigroup theory to certain partial differential equations. In Michael G. Crandall, editor, *Nonlinear Evolution Equations*, pages 163–188. Academic Press, 1978.
- [20] Y. Gao, G. Yuan, S. Wang, and X. Hang. A finite volume element scheme with a monotonicity correction for anisotropic diffusion problems on general quadrilateral meshes. *J. Comput. Phys.*, 407:109143, 2020.
- [21] Z. Gao and J. Wu. A second-order positivity-preserving finite volume scheme for diffusion equations on general meshes. *SIAM J. Sci. Comput.*
- [22] G. H. Golub and C. F. Van Loan. *Matrix Computations (3rd Ed.)*. Johns Hopkins University Press, USA, 1996.
- [23] M. Käser and A. Iske. Ader schemes on adaptive triangular meshes for scalar conservation laws. *J. Comput. Phys.*, 205(2):486–508, 2005.
- [24] E. Labourasse. *Contribution to the numerical simulation of radiative hydrodynamics*. Habilitation à diriger des recherches, sorbonne university, December 2021.
- [25] O. Larroche. An efficient explicit numerical scheme for diffusion-type equations with a highly inhomogeneous and highly anisotropic diffusion tensor. *J. Comput. Phys.*, 223:436–450, 2007.
- [26] C. Le Potier. Schéma volumes finis monotone pour des opérateurs de diffusion fortement anisotropes sur des maillages de triangles non structurés. *C. R. Math.*, 341(12):787–792, 2005.
- [27] P.-H. Maire. A high-order cell-centered Lagrangian scheme for two-dimensional compressible fluid flows on unstructured meshes. *J. Comput. Phys.*, 228(7):2391–2425, 2009.

- [28] G. Meurant. *Computer solution of large linear systems*. Elsevier, 1999.
- [29] R.J. Plemmons. m-matrix characterizations.i – nonsingular m-matrices. *Linear Algebra and its Applications*, (2):175 – 188.
- [30] E. H. Quenjel. Enhanced positive vertex-centered finite volume scheme for anisotropic convection-diffusion equations. *ESAIM, Math. Model. Numer. Anal.*, 54(2):591–618, 2020.
- [31] L. Rebholz and M. Xiao. The effect of anderson acceleration on superlinear and sublinear convergence. *J. Sci. Comput.*, 96, 06 2023.
- [32] Z. Sheng and G. Yuan. A new nonlinear finite volume scheme preserving positivity for diffusion equations. *J. Comput. Phys.*, 315:182–193, 2016.
- [33] R. S. Varga. *Matrix iterative analysis*, volume 1. Prentice Hall, 1962.
- [34] J. Wang, Z. Sheng, and G. Yuan. A finite volume scheme preserving maximum principle with cell-centered and vertex unknowns for diffusion equations on distorted meshes. *Appl. Math. Comput.*, 398(1):1–21, 2021.
- [35] S. Wang and G. Yuan. Discrete strong extremum principles for finite element solutions of diffusion problems with nonlinear corrections. *Appl. Numer. Math.*, 174:1–16, 2022.
- [36] J. Wu and Z. Gao. Interpolation-based second-order monotone finite volume schemes for anisotropic diffusion equations on general grids. *J. Comput. Phys.*, 275:569–588, 2014.
- [37] H. Yang, B. Yu, Y. Li, and G. Yuan. Monotonicity correction for second order element finite volume methods of anisotropic diffusion problems. *J. Comput. Phys.*, 449:110759, 2022.
- [38] G. Yuan and Z. Sheng. Monotone finite volume schemes for diffusion equations on polygonal meshes. *J. Comput. Phys.*, 227(12):6288–6312, 2008.
- [39] X. Zhang, S. Su, and J. Wu. A vertex-centered and positivity-preserving scheme for anisotropic diffusion problems on arbitrary polygonal grids. *J. Comput. Phys.*, 344:419–436, 2017.
- [40] F. Zhao, Z. Sheng, and G. Yuan. A monotone combination scheme of diffusion equations on polygonal meshes. *Z. Angew. Math. Mech.*, 100(5):1–25, 2020.